Chemosphere 95 (2014) 9–16

Contents lists available at SciVerse ScienceDirect

Chemosphere

journal homepage: www.elsevier.com/locate/chemosphere

Source and mixing state of iron-containing particles in Shanghai by individual particle analysis

Guohua Zhang [a,b], Xinhui Bi [a,*], Shengrong Lou [c], Lei Li [d], Hongli Wang [c], Xinming Wang [a], Zhen Zhou [d], Guoying Sheng [a], Jiamo Fu [a,d], Changhong Chen [c,*]

[a] State Key Laboratory of Organic Geochemistry, Guangzhou Institute of Geochemistry, Chinese Academy of Sciences, Guangzhou 510640, PR China
[b] Graduate University of Chinese Academy of Sciences, Beijing 100049, PR China
[c] Shanghai Academy of Environmental Sciences, Shanghai 200233, PR China
[d] School of Environmental and Chemical Engineering, Shanghai University, Shanghai 200444, PR China

HIGHLIGHTS

- Number fraction of Fe-containing particles varied from <1% to 15%.
- Fe-containing particles in Shanghai most correspond to anthropogenic sources.
- Dust is suspected to be more responsible for the spike of Fe-containing particles.
- Anthropogenic Fe aerosol tended to associate with secondary species.

ARTICLE INFO

Article history:
Received 23 January 2013
Received in revised form 11 April 2013
Accepted 13 April 2013
Available online 26 May 2013

Keywords:
Iron-containing particles
Individual particle
Source
Mixing state
SPAMS

ABSTRACT

Bioavailable iron (Fe) is an essential nutrient that can control oceanic productivity, thereby impacting the global carbon budget and climate. Therefore it is of vital importance to identify chemical species and mixing state of Fe-containing particles in the air, which are demonstrated to pose substantial impact on bioavailability of Fe. Using a single particle aerosol mass spectrometer (SPAMS), ~2 000 000 individual particles with mass spectra were collected in Shanghai for nearly 22 d during the winter of 2011. Number fraction of Fe-containing particles (Nf_{Fe}) varied in a wide range (<1–15%) throughout the measurement. Fe-containing particles were mainly clustered into four chemical groups, comprising of Fe-rich, K-rich, Dust and V-containing particle types. Analysis of mass spectra and mixing state suggests that Fe-containing particles correspond to various sources in Shanghai, especially anthropogenic sources iron/steel industrial activities, and fly ashes from both biomass burning and coal combustion, accounting for ~55% and ~18%, respectively. However, invasion of dust from northern desert areas is suspected to be more responsible for the spikes of Nf_{Fe} (>10%), when Dust particle type contributed to >50% of Fe-containing particles. It is also revealed that Fe-containing particles were internally mixed with secondary species (e.g., sulfate and nitrate). Anthropogenic K-rich and Fe-rich particles tended to associate with both sulfate and nitrate, and thus might lead to more fraction of soluble Fe, compared to Dust particles. These results imply that atmospheric processing of Fe-containing particles from various sources might vary and thus would change the bioavailability of atmospheric Fe.

1. Introduction

As the dominant species of the transition metals in the atmosphere, iron (Fe) substantially impacts human health, atmospheric physics and chemistry, and bioavailability to marine ecosystem (Prahalad et al., 2001). Atmospheric Fe associates with adverse health effects due to mechanisms such as DNA strand breakage and tissue or cell damage (See et al., 2007). Fe influences on the optical property of mineral dust (Moosmüller et al., 2012), and also is involved in the atmospheric conversion of S(IV) to S(VI), a substantial pathway for global atmospheric sulfate production (Alexander et al., 2009). Furthermore, atmo-

* Corresponding authors. Tel.: +86 20 85290195; fax: +86 20 85290288 (X. Bi), tel.: +86 21 64085119; fax: +86 21 54641938 (C. Chen).
E-mail addresses: bixh@gig.ac.cn (X. Bi), chench@saes.sh.cn (C. Chen).

0045-6535/$ - see front matter © 2013 Elsevier Ltd. All rights reserved.
http://dx.doi.org/10.1016/j.chemosphere.2013.04.046

spheric Fe plays an important role in the global carbon cycle through effects on marine productivity that is expected to have feedback effects on climate and dust production (Mahowald et al., 2005).

Aerosol Fe solubility varies in a wide range and therefore it represents the major uncertainty in its impacts as aforementioned (Mahowald et al., 2009). It had been reported that Fe solubility from various sources is diverse, spanning four orders of magnitude (Schroth et al., 2009). The soluble fraction of Fe in Chinese desert soil was ~0.4 ± 0.3% (Zhuang et al., 1992), however, aerosol Fe solubility heterogeneously distributes in space and time (0.001–80%) (Mahowald et al., 2005; Ooki et al., 2009). Natural emissions represent the predominant sources of atmospheric Fe, accounting for 70–80% (Jickells et al., 2005). However, recent studies highlight the important role of industrial activities, coal combustion and biomass burning in the increased soluble aerosol Fe (Guieu et al., 2005; Chen et al., 2012). Although combustion sources are not important for the total Fe mass compared to natural sources, they can contribute up to 50% of soluble Fe deposited into oceanic regions (Luo et al., 2008).

A variety of atmospheric processes, including photochemistry, organic complexion, and in particular cloud processing, can influence aerosol Fe speciation and its solubility. It had been well-documented that aerosol acidification involving urban pollutants plays a substantial role in the increase of soluble Fe (Rubasinghege et al., 2010). Many studies attempted to investigate the correlation between aerosol Fe fractional solubility and concentrations of acid species (Hand et al., 2004; Baker et al., 2006), in order to interpret a potential link between acid processing and Fe solubility. However, Baker and Croot (2010) emphasized the conformation of physical contact between Fe and acidic compounds on the exactly same particles, even if acid processing is the primary atmospheric control of the Fe fractional solubility. Aerosol Fe mixing state, referring to the association of Fe with various species such as sulfate, organics and nitrate, is the net result of primary emissions as well as subsequent atmospheric chemical and physical processes, and thus it represents one of the most controlling factors that affect aerosol Fe solubility (Baker and Croot, 2010; Chen et al., 2012). Therefore, knowledge on the sources and mixing state of aerosol Fe is a necessity and it helps to understand the effect of aerosol Fe on the marine productivity and global climate change.

Located near the East China Sea, Shanghai develops with many industries, such as Iron & Steel and petrochemical complex, which might be associated with frequently observed high aerosol loadings (Fu et al., 2008). Single particle mass spectrometer has been applied to study the sources and the formation mechanisms of aerosols in the atmosphere of Shanghai (e.g., Zhang et al., 2009). Using the similar technique, Furutani et al. (2011) found the importance of coal combustion source to the strength of Fe aerosols in China mainland. To date, only a few studies have focused on aerosol Fe in Shanghai (Wang et al., 2006, 2013), despite of their substantial impact on not only the air quality of Shanghai, but also the productivity of nearby waters (e.g., the Yellow sea).

In this study, a single particle aerosol mass spectrometer (SPAMS) was employed during the winter of 2011 in urban Shanghai to determine both the size and chemical composition of individual atmospheric particles, with vacuum aerodynamic diameter (d_{va}) in the size range of 0.2–2 μm. Air masses originating from the northern desert region arriving Shanghai during the winter provided an opportunity to directly observe the mixing of Fe-containing particles from both anthropogenic and natural sources with anthropogenic pollutants. A large set of single particle mass spectra was collected and analyzed in order to identify the origin and mixing state of Fe-containing particles.

2. Experiment setup

2.1. Atmospheric observations

Ambient aerosol measurement was conducted in Shanghai Academy of Environmental Sciences (SAESs), located in the center of urban Shanghai, between 9th and 31st December 2011 using a SPAMS, manufactured by Hexin Analytical Instrument Co., Ltd. (Guangzhou, China). The sampling site location with a detailed map of Shanghai industrial area, and a wind-rose for the entire measurement period are presented in Fig. S1 in Supplementary material (SM). The inlet of the sampling tube was set at 2 m above the roof of the Atmospheric Environment Monitoring Building of SAES. Local meteorological parameters, including ambient temperature (T, °C), relative humidity (RH, %), and wind speed (WS, m s^{-1}), were available from Weather Underground (http://www.wunderground.com/), and temporal profiles of these parameters are shown in Fig. S2. Ambient T, RH, and WS during the field study varied between −2 and 13 °C, 25–100%, and 0–9 m s^{-1}, with average values of 5.5 °C, 63%, and 3.8 m s^{-1}, respectively.

Single particles detection method was described in detail in the SM. Regarding the strong dependence of particle detection efficiency on particle size and chemical components by SPAMS (Su et al., 2004), the particle counts and number fraction applied in this study only provided an indication of their relative abundance, rather than the absolute concentration.

2.2. Screening and clustering of Fe-containing particles

During the winter sampling period, a total of approximate 2 000 000 particles, with d_{va} between 0.2 and 2.0 μm, were chemically analyzed with positive and negative ion mass spectra. Fe-containing particles commonly produce an intense ion peak at mass-to-charge ratio (m/z) 56 in the positive ion mass spectrum. However, simply using ion peak at m/z 56 as a unique marker for Fe is not suitable, since it might be also generated in the form of CaO^+, KOH^+, and $C_3H_4O^+$ from other components. Therefore, the natural isotopic composition of Fe (^{54}Fe) was selected for the Fe screening process to minimize the interference from other species. The isotopic ratio of Fe ($^{56}Fe/^{54}Fe = 16$) was commonly used as a marker for Fe, although it is set relatively flexible, such as Peak-Area ratio $^{56}Fe/^{54}Fe > 3$ in Furutani et al. (2011), due to the variation of the ratio resulted from the matrix effect of laser desorption/ionization (Allen et al., 2000). In this study, all the possible Fe particles, referring to the particles contained both peaks from ^{56}Fe and ^{54}Fe, were separated into two fractions: particles with Peak-Area ratio $^{56}Fe/^{54}Fe > 10$ and <10, respectively. Indeed, the average mass spectrum of the particles with $^{56}Fe/^{54}Fe < 10$ resembled that of organic carbon, characterized by the obvious organic peaks at m/z 27$[C_2H_3]^+$, 29$[C_2H_5]^+$, 43$[C_2H_3O]^+$, 51$[C_4H_3]^+$, 63$[C_5H_3]^+$, 77$[C_6H_5]^+$ and 91$[C_7H_7]^+$ (Dall'Osto and Harrison, 2012). Therefore, Peak-Area ratio $^{56}Fe/^{54}Fe > 10$ was finally applied to strengthen the screening through excluding more ambiguous selection.

The screened Fe-containing particles were subsequently analyzed using an adaptive resonance theory based neural network algorithm (ART-2a) (Song et al., 1999), with a vigilance factor of 0.8, learning rate of 0.05, and 20 iterations. The chemical compositions of the produced clusters resulted from ART-2a were carefully examined to identify whether these clusters corresponded to the assignment of Fe. A few clusters characterized by relative high OC peaks (m/z 27, 37, 43) and low intensity at m/z 56, representing less than 5% of the total screened particles, were not likely to be the Fe-containing particle types. Therefore, they were excluded from the screened Fe-containing particles to avoid the ambiguous assignment.

3. Results and discussion

3.1. Mass spectral characteristic of Fe-containing particles

Number fraction of each ion peak present in Fe-containing particles is displayed in Fig. 1. Dominant peaks in the positive ion mass spectrum were Fe (54/56[Fe]$^+$), K (39[K]$^+$), and Na (23[Na]$^+$). Many other peaks attributed to primary species, such as m/z 7[Li]$^+$, 24[Mg]$^+$, 27[Al]$^+$, 40[Ca]$^+$, 48[Ti]$^+$/64[TiO]$^+$, 51[V]$^+$/67[VO]$^+$, −76[SiO_3]$^-$, and −79[PO_3]$^-$, also coexisted with Fe. They are valuable for source elucidation of Fe-containing particles. Almost all observed Fe-containing particles associated with secondary species, such as ammonium (18[NH_4]$^+$), nitrate (−46[NO_2]$^-$, −62[NO_3]$^-$, −125[$H(NO_3)_2$]$^-$), and/or sulfate (−97[HSO_4]$^-$, −80[SO_3]$^-$), which indicates that Fe-containing particles experienced atmospheric physicochemical processing during atmospheric transport. Frequent existence of m/z 72, 73, and 90 in Fe-containing particles were most probably assigned to be 72[FeO]$^+$, 73[FeOH]$^+$, and 90[$Fe(OH)_2$]$^+$, respectively. Other ion peaks corresponding to Fe such as 112[Fe_2]$^+$, 128[Fe_2O]$^+$, −88[FeO_2]$^-$ and −104[FeO_3]$^-$ were also observed. The higher number fraction of these iron oxides in Fe-containing particles, comparing with other detected particles (Fig. S3), indicates the accumulation of iron oxide clusters in Fe-containing particles (Yan et al., 2010).

3.2. Single particle types of Fe-containing particles

Size-resolved (in 100 nm resolution) number distribution and number fraction, and temporal variation (in 1 h resolution) of Fe-containing particles are shown in Fig. S4. Fe-containing particles (64371 in total number) contributed approximately 3.3% on average to all detected particles in a wide range (<1–15%) throughout the sampling period. Size-resolved number fraction of Fe-containing particles (Nf_{Fe}) varied between 2.6% and 4.6%, generally lower values in submicron particles and higher values in super-micron particles. The maximum value (4.6%) was obtained around the d_{va} of 1.4–1.5 μm. Table S1 lists four different single particle types by ART-2a representing a major chemical association of Fe-containing particles. The average mass spectra of these four particle types are provided in Fig. S5, and their characteristics are briefly described in the following text.

Fe-rich particles represented the largest fraction (~55%) of Fe-containing particles. These particles contained Fe ion peak as the most intense peak of their mass spectra, with relatively weak K and Na peaks. It might suggest that this particle type contained Fe as a main metallic component, regarding that other frequently observed atmospheric metals such as K, Na, Li, Al, and Ca have higher first ionization potential than Fe (http://www.tannerm.com), and that the relative sensitivity factors of different elements detected by laser desorption/ionization based mass spectrometry are strongly dependent on first ionization potential (Gross et al., 2000). Dust particle type was the secondary contributor, accounting for ~25% of Fe-containing particles. Mass spectra of the particles showed that the major peaks were K (m/z 39), Na (m/z 23), Fe (m/z 56), Al (m/z 27), Ca (m/z 40). Peaks for other metals such as Mg (m/z 24) and Ti (m/z 48 and 64) can also be seen in the mass spectra. Its negative mass spectra showed ions from O/OH (m/z −16/−17), Cl (m/z −35/−37), silicate (m/z −60/−76), and nitrate (m/z −46/−62). K-rich particle type, characterized by the intense peaks of 39[K]$^+$ and 23[Na]$^+$ besides that of 56[Fe]$^+$, contributed ~18% to Fe-containing particles. In addition, other peaks correspond to carbonaceous compositions (−26[CN]$^-$, 27[C_2H_3]$^+$, 12[C]$^+$, 36[C_3]$^+$, 37[C_3H]$^+$) were also frequently detected. V-containing particle type only accounted for a negligible fraction (~2%) of Fe-containing particles. It was characterized by the unique presence of V ion peaks (m/z 51[V]$^+$, m/z 67[VO]$^+$), with frequent association of Al and Ni ion peaks.

3.3. Possible sources for Fe-containing particles

The mixing state of Fe-containing particle types with primary and secondary markers, together with iron oxide clusters as aforementioned, and the temporal variation (in 1 h resolution) of num-

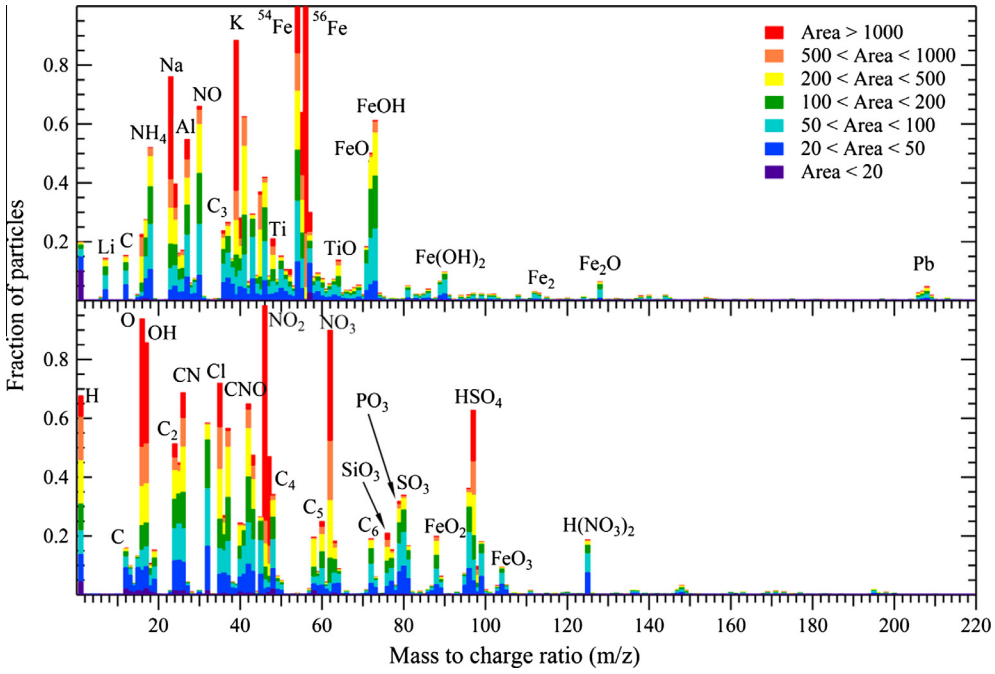

Fig. 1. Average positive (top) and negative (bottom) digitized mass spectrum of Fe-containing particles over the wintertime sampling. y-Axis represents the number fraction of each ion in Fe-containing particles. The coloration indicates the absolute intensity of each ion.

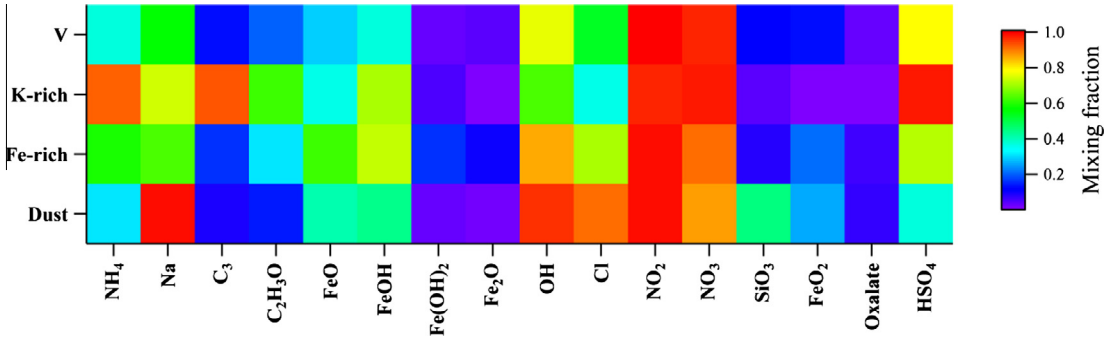

Fig. 2. Mixing state of primary and secondary markers on the various Fe-containing particle types. The color scaled represents the number fraction of Fe-containing particle types that contained the corresponding markers.

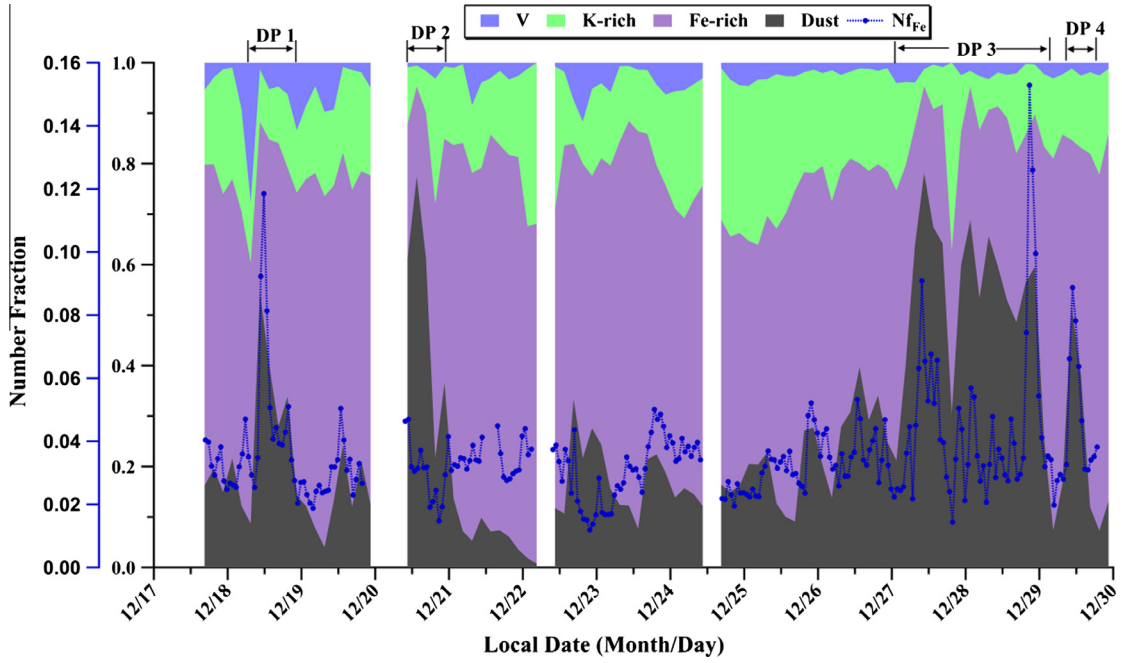

Fig. 3. Temporal profiles of number fraction of Fe-containing particle types relative to all the Fe-containing particles, and Nf_{Fe} relative to all the detected particles during 17–31 December 2011.

ber fraction of these particle types are shown in Figs. 2 and 3, respectively. The markers were selected mainly according to the previous documentation (Moffet et al., 2008) and listed in Table S2. In addition, the air mass back-trajectories simulated by HYSPLIT (in the SM) were clustered and generated four major groups, to further reveal their influence on the Fe-containing particle types of Shanghai in winter season. The four major clusters of air mass trajectories, number fraction of Fe-containing particle types for each air mass cluster, and potential sources estimated by PSCF (in the SM) are illustrated in Fig. 4. Over the course of this study, the urban Shanghai site was under the influence of air masses from northern dust areas, including north-eastern deserts (cluster 1), Mongolian (Northern Gobi) deserts (cluster 2), and Inner Mongolian (Southern Gobi) deserts (clusters 3 and 4).

Regarding that Fe-containing particles emitted from iron/steel industry are commonly iron oxides formed through industrial high-temperature processes (Flament et al., 2008), the Fe-rich particles in the present study were more likely to be produced by iron/steel industry, which is consistent with the finding that the iron oxides enriched in the Fe-rich particles (Fig. 2). These oxides are usually interpreted as goethite (FeO(OH)), hematite (Fe_2O_3) or magnetite (Fe_3O_4) in the atmospheric aerosols (Wang et al., 2006; Elzinga et al., 2011). Using scanning electron microscopy coupled with energy analysis (SEM–EDX), Yue et al. (2006) showed that high concentration of Fe aerosol was related to metallurgical emissions. As also observed in urban Shanghai and air mass from mainland China by single particle mass spectrometry, this particle type was similarly attributed to metallurgic emissions from the steel manufacturing and processing facilities (Zhang et al., 2009; Furutani et al., 2011). As illustrated in Fig. S1, the predominant wind from northern areas of the sampling site brought in pollutants from industrial areas, where Bao Steel Group, one of the most important metallurgical enterprises of China, and some other metallurgical factories such as the Shanghai No. 1 Steel Plant are located. The temporal variation showed that this particle type was generally the dominant Fe-containing particle type in the atmospheric aerosol of Shanghai, and their number fraction was relatively stable throughout the field study (Fig. 3), except dust invasion periods (discussed in following text). This result might also serve as an indication of the local industry emissions.

K-rich particle type was attributed to fly ashes from combustion activities, such as coal combustion and/or biomass burning activi-

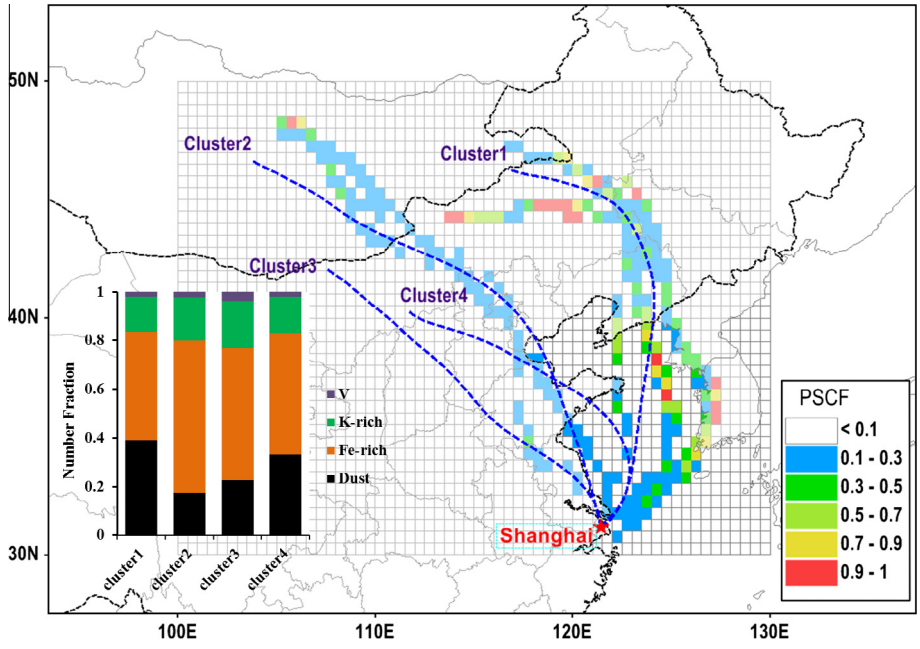

Fig. 4. Four major clusters for air mass trajectories (in dash line), number fraction of Fe-containing particle types for each air mass cluster (in the bar plot), and probabilities for potential sources of Fe-containing particles estimated by PSCF (in color grid). (For interpretation of the references to color in this figure legend, the reader is referred to the web version of this article.)

ties. Intense 39[K]$^+$ peak coupled with carbonaceous ion peaks is commonly utilized as an indicator of biomass/biofuel origin (Pratt et al., 2011). Note that the carbonaceous ion markers (36[C_3]$^+$ and/or 43[C_2H_3O]$^+$) were found most and exclusively in these particles (Fig. 2). Similar chemical components in fine aerosols from the anthropogenic sources were also observed in the air masses from South-East Asia continent (Kumar et al., 2010). In addition, the presence of Li (7[Li]$^+$) suggests the origin of fly ashes from coal combustion (Guazzotti et al., 2003). Previous researches revealed that Li is seldom detected in the single particles released from biomass/biofuel burning (<0.3%) (Silva et al., 1999), but frequently observed in particles emitted from coal combustion (Guazzotti et al., 2003). In this study, Li was present in ~11% of these K-rich particles, which might provide a conservative estimation of the contribution from coal combustion, mainly from power plant and industrial processes (Huang et al., 2011). Inconsistent with the finding by Furutani et al. (2011) that this particle type represented the most abundant fraction (~50%) of Fe-containing particles in air mass from mainland China, our finding showed that Fe-rich was the dominant type (~55%), rather than K-rich (~18%). This discrepancy might be attributed to the influence of local emission in Shanghai that dominantly produced Fe-rich.

Dust particle type exhibited mostly the ion peaks associated with Al, Ca, and Ti elements in the positive mass spectra, representing the dust aerosols (Arimoto et al., 2006). It is in accordance with the analysis that silicate (a marker for the dust origin) was exclusively associated with this particle type (Fig. 2). It is also worth noting that during the field study, the number fraction of Dust particles (Nf_{Dust}) showed four major spikes (marked as DP in Fig. 3), when it increased sharply to larger than 50%. The particles during DP1, DP2, DP3 and DP4 represented ~40–70% of super-micron (1.0–2.0 μm) Fe-containing particles, compared to ~23% on average throughout the study. Meanwhile, Nf_{Fe} also increased considerably during each DP, and it even exceeded 10% of all detected particles for DP1, DP3, and DP4, however, not for DP2. The simulated air mass back-trajectories from HYSPLIT 4.9 supported the impact of dust Fe from long range transport. Clusters 1 and 4 transported through the marine regions, whereas clusters 2 and 3 were mainly contributed by continental emitted pollutants. As estimated by the PSCF, areas around cluster 1 were the main transport passage with the highest probability that resulted in the spikes of Fe-containing particles, mainly through the importing of Fe in the dust aerosol. The dust particle type associated with the cluster 1 accounted for ~40% of Fe-containing particles. It is noted that the cluster 4 also transported through the passages of cluster 1 and thus it carried larger fraction of dust. Compared to the clusters 1 and 4 through marine regions, the clusters 2 and 3 brought relatively higher fraction of anthropogenic Fe-containing particles (i.e., Fe-rich and K-rich) from polluted continental regions. The contribution of Dust particle type to the spike of Nf_{Fe} is further supported by the correlation analysis between Nf_{Dust} and Nf_{Fe} during four DPs (Fig. S6) as discussed in the SM.

V-containing particles were primarily attributed to residual fuel oil combustion, associated with sources such as ships and refineries (Ault et al., 2010), which should be true for Shanghai, since it was a coastal mega-city with relatively high loading of shipments.

3.4. Mixing state of Fe-containing particles with secondary inorganic species

As aforementioned, the association of Fe-containing particles with secondary inorganic species was common during this study, however, they might show different mixing patterns (Fig. 2). Nitrate showed a predominant fraction (>85% in number fraction) in all the particle types, while sulfate and ammonium were observed mostly associated with K-rich particles (~98% and ~92%, respectively). Fresh biomass burning particles are generally hygroscopic, and thus are expected to be favorable for the formation of sulfate and nitrate (Pratt et al., 2011). However, Dust particles might contain higher fraction of water insoluble compounds (e.g., silicate) and therefore uptake of SO_2 would be relatively slow, resulting in the least fraction of sulfate. SO_2 does not contain acidic protons unless it is hydrated and oxidized, while HNO_3 can be readily neutralized upon reactions with these alkaline species (Sullivan et al., 2007). Yang and Gao (2007) suggested that coating by HNO_3 can more effectively produce soluble Fe fluxes compared

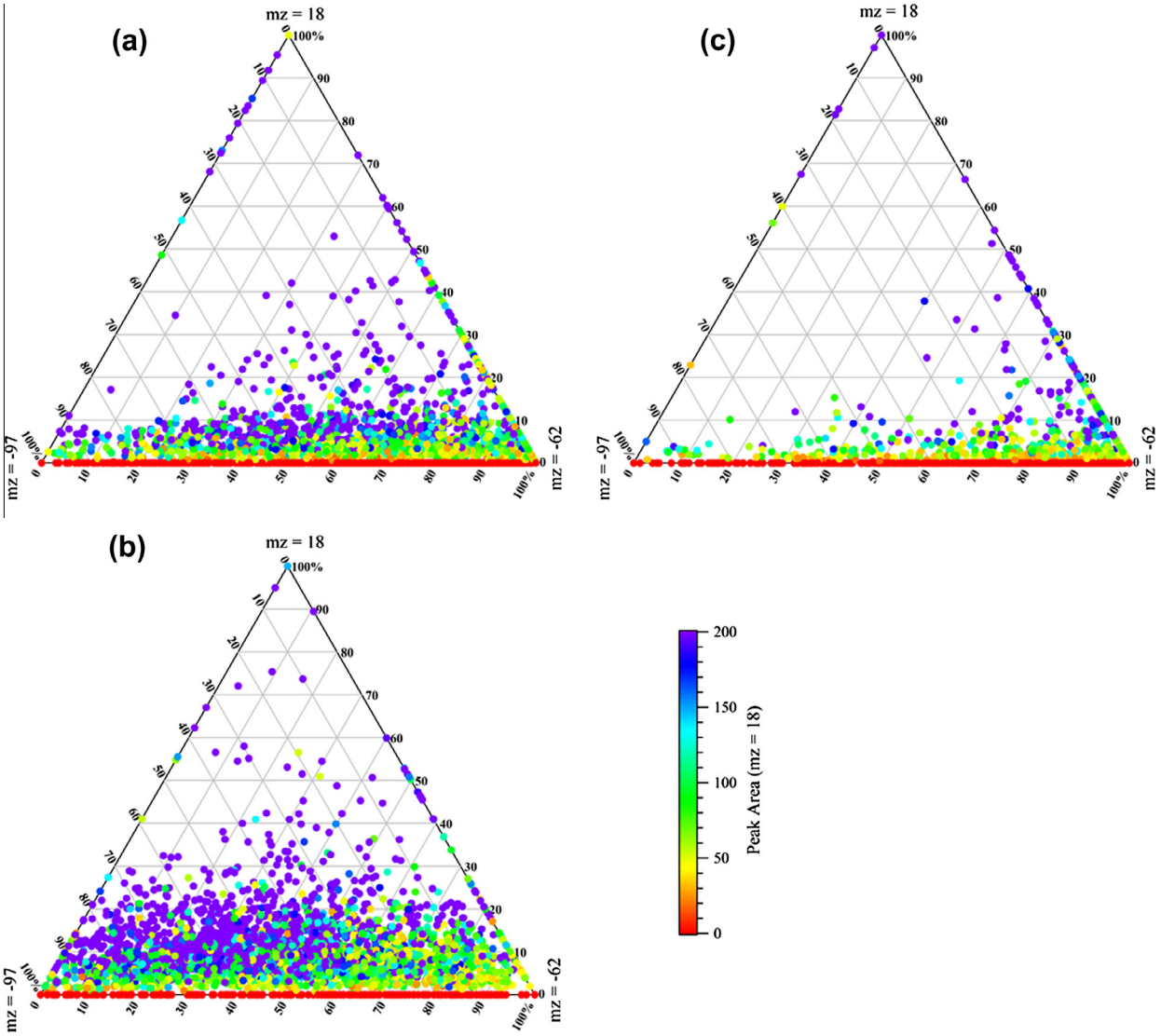

Fig. 5. Ternary plot of peak intensities for secondary inorganic species (i.e., sulfate, nitrate, and ammonium) in (a) Fe-rich, (b) K-rich, and (c) Dust particle type, respectively. The color dots indicate the peak areas of ammonium in the particles. 3000 particles were randomly selected for the comparison. In a ternary plot, a particle containing primarily sulfate relative to ammonium and nitrate would appear at the left vertex, primarily ammonium at the top vertex, and nitrate would appear at the right vertex.

to those by SO_2 and sulfate. Compared to K-rich and Dust particles, Fe-rich particles contained moderate fraction of these species. These results might lead to a conclusion that uptake of SO_2 and/or HNO_3 on Fe-containing particles links to their chemical compositions, or particle types.

The above discussion, based on the particle number count, was also supported by the ion intensity analysis which was commonly applied to access the relative amount of individual species (Sullivan et al., 2007). As illustrated in Fig. 5, the peak intensity distribution of ammonium, nitrate and sulfate in three particle types further demonstrates the diversities of these species associated with Fe-containing particles. The dots for both Fe-rich and K-rich particle types distributed along the nitrate and sulfate, however, they mainly appeared at the right vertex for Dust particles. The distribution indicates that Fe-rich and K-rich particle types associated with both sulfate and nitrate, while Dust particles contained nitrate as the primarily secondary species. Saharan dust particles observed near the Cape Verde Islands also showed increased internally mixed nitrate but no sulfate, through the application of single particle measurements (Dall'Osto et al., 2010). This result indicates that the presence of ammonium nitrate and/or ammonium sulfate in all these particle types was negligible since few dots distributed along the axis of ammonium and sulfate/nitrate. The limited content of ammonium in these particle types might further indicate the association of secondary acids with alkali components other than ammonium. Uptake of acidic coatings should result in a considerable increase of soluble Fe in the atmospheric aerosols (Baker and Croot, 2010). These facts provide further evidence that different single particle types of Fe-containing particles from various sources could possibly be responsible for the diversities of their mixing state with acidic species, and as a consequence, different Fe solubility.

4. Conclusion

Size and chemical composition of individual atmospheric Fe-containing aerosols with d_{va} between 0.2 and 2 μm during the winter were characterized in urban Shanghai. Their mass spectral

characteristic, temporal profiles, and mixing state were analyzed, and the obtained major conclusions are listed as follows.

(1) Anthropogenic Fe-containing aerosols (Fe-rich from iron/steel industrial activities, K-rich from biomass burning/coal combustion) represent the most important fraction of Fe-containing particles in Shanghai atmosphere.
(2) Invasion of dust from the northern desert regions might be the reason for the spike of Nf_{Fe}.
(3) Fe-containing particles were shown to be internally mixed with secondary species, whereas the extent varies.
(4) Single particle compositions may influence their mixing state with secondary acidic species, and therefore the solubility.

To the extent that soluble Fe acts as a limiting micronutrient in oceanic ecosystems, Fe exhausted from anthropogenic pollution should be considered for enhancing the productivity of nearby waters, in addition to local health problem related air quality.

Acknowledgements

We would like to thank all participants for atmospheric sampling at Shanghai Academy of Environmental Sciences. This work was supported by the National Nature Science Foundation of China (No. 41073077), "Strategic Priority Research Program (B)" of the Chinese Academy of Sciences (Grant No. XDB05020205), and Guangzhou Institute of Geochemistry (GIGCAS 135 Project Y234161001). The authors also gratefully acknowledge the NOAA Air Resources Laboratory (ARL) for the provision of the HYSPLIT transport and dispersion model and/or READY website (http://ready.arl.noaa.gov) used in this publication. This is contribution No. 1668 from GIGCAS.

Appendix A. Supplementary material

Supplementary data associated with this article can be found, in the online version, at http://dx.doi.org/10.1016/j.chemosphere.2013.04.046.

References

Alexander, B., Park, R.J., Jacob, D.J., Gong, S.L., 2009. Transition metal-catalyzed oxidation of atmospheric sulfur: global implications for the sulfur budget. J. Geophys. Res.-Atmos. 114, D02309.
Allen, J.O., Fergenson, D.P., Gard, E.E., Hughes, L.S., Morrical, B.D., Kleeman, M.J., Gross, D.S., Galli, M.E., Prather, K.A., Cass, G.R., 2000. Particle detection efficiencies of aerosol time of flight mass spectrometers under ambient sampling conditions. Environ. Sci. Technol. 34, 211–217.
Arimoto, R., Kim, Y.J., Kim, Y.P., Quinn, P.K., Bates, T.S., Anderson, T.L., Gong, S., Uno, I., Chin, M., Huebert, B.J., Clarke, A.D., Shinozuka, Y., Weber, R.J., Anderson, J.R., Guazzotti, S.A., Sullivan, R.C., Sodeman, D.A., Prather, K.A., Sokolik, I.N., 2006. Characterization of Asian Dust during ACE-Asia. Glob. Planet. Change 52, 23–56.
Ault, A.P., Gaston, C.J., Wang, Y., Dominguez, G., Thiemens, M.H., Prather, K.A., 2010. Characterization of the single particle mixing state of individual ship plume events measured at the port of Los Angeles. Environ. Sci. Technol. 44, 1954–1961.
Baker, A.R., Croot, P.L., 2010. Atmospheric and marine controls on aerosol iron solubility in seawater. Mar. Chem. 120, 4–13.
Baker, A.R., French, M., Linge, K.L., 2006. Trends in aerosol nutrient solubility along a west–east transect of the Saharan dust plume. Geophys. Res. Lett. 33, L07805.
Chen, H., Laskin, A., Baltrusaitis, J., Gorski, C.A., Scherer, M.M., Grassian, V.H., 2012. Coal fly ash as a source of iron in atmospheric Dust. Environ. Sci. Technol. 46, 2112–2120.
Dall'Osto, M., Harrison, R.M., 2012. Urban organic aerosols measured by single particle mass spectrometry in the megacity of London. Atmos. Chem. Phys. 12, 4127–4142.
Dall'Osto, M., Harrison, R.M., Highwood, E.J., O'Dowd, C., Ceburnis, D., Querol, X., Achterberg, E.P., 2010. Variation of the mixing state of Saharan dust particles with atmospheric transport. Atmos. Environ. 44, 3135–3146.
Elzinga, E.J., Gao, Y., Fitts, J.P., Tappero, R., 2011. Iron speciation in urban dust. Atmos. Environ. 45, 4528–4532.
Flament, P., Mattielli, N., Aimoz, L., Choël, M., Deboudt, K., Jong, J.d., Rimetz-Planchon, J., Weis, D., 2008. Iron isotopic fractionation in industrial emissions and urban aerosols. Chemosphere 73, 1793–1798.
Fu, Q., Zhuang, G., Wang, J., Xu, C., Huang, K., Li, J., Hou, B., Lu, T., Streets, D.G., 2008. Mechanism of formation of the heaviest pollution episode ever recorded in the Yangtze River Delta, China. Atmos. Environ. 42, 2023–2036.
Furutani, H., Jung, J., Miura, K., Takami, A., Kato, S., Kajii, Y., Uematsu, M., 2011. Single-particle chemical characterization and source apportionment of iron-containing atmospheric aerosols in Asian outflow. J. Geophys. Res. 116, D18204.
Gross, D.S., Galli, M.E., Silva, P.J., Prather, K.A., 2000. Relative sensitivity factors for alkali metal and ammonium cations in single particle aerosol time-of-flight mass spectra. Anal. Chem. 72, 416–422.
Guazzotti, S.A., Suess, D.T., Coffee, K.R., Quinn, P.K., Bates, T.S., Wisthaler, A., Hansel, A., Ball, W.P., Dickerson, R.R., Neususs, C., Crutzen, P.J., Prather, K.A., 2003. Characterization of carbonaceous aerosols outflow from India and Arabia: biomass/biofuel burning and fossil fuel combustion. J. Geophys. Res.-Atmos. 108, D15.
Guieu, C., Bonnet, S., Wagener, T., Loye-Pilot, M.D., 2005. Biomass burning as a source of dissolved iron to the open ocean? Geophys. Res. Lett. 32, L19608.
Hand, J.L., Mahowald, N.M., Chen, Y., Siefert, R.L., Luo, C., Subramaniam, A., Fung, I., 2004. Estimates of atmospheric-processed soluble iron from observations and a global mineral aerosol model: biogeochemical implications. J. Geophys. Res.-Atmos. 109, D17205.
Huang, C., Chen, C.H., Li, L., Cheng, Z., Wang, H.L., Huang, H.Y., Streets, D.G., Wang, Y.J., Zhang, G.F., Chen, Y.R., 2011. Emission inventory of anthropogenic air pollutants and VOC species in the Yangtze River Delta region, China. Atmos. Chem. Phys. 11, 4105–4120.
Jickells, T.D., An, Z.S., Andersen, K.K., Baker, A.R., Bergametti, G., Brooks, N., Cao, J.J., Boyd, P.W., Duce, R.A., Hunter, K.A., Kawahata, H., Kubilay, N., laRoche, J., Liss, P.S., Mahowald, N., Prospero, J.M., Ridgwell, A.J., Tegen, I., Torres, R., 2005. Global iron connections between desert dust, ocean biogeochemistry, and climate. Science 308, 67–71.
Kumar, A., Sarin, M.M., Srinivas, B., 2010. Aerosol iron solubility over Bay of Bengal: role of anthropogenic sources and chemical processing. Mar. Chem. 121, 167–175.
Luo, C., Mahowald, N., Bond, T., Chuang, P.Y., Artaxo, P., Siefert, R., Chen, Y., Schauer, J., 2008. Combustion iron distribution and deposition. Glob. Biogeochem. Cycle 22, GB1012.
Mahowald, N.M., Baker, A.R., Bergametti, G., Brooks, N., Duce, R.A., Jickells, T.D., Kubilay, N., Prospero, J.M., Tegen, I., 2005. Atmospheric global dust cycle and iron inputs to the ocean. Glob. Biogeochem. Cycle 19, GB4025.
Mahowald, N.M., Engelstaedter, S., Luo, C., Sealy, A., Artaxo, P., Benitez-Nelson, C., Bonnet, S., Chen, Y., Chuang, P.Y., Cohen, D.D., Dulac, F., Herut, B., Johansen, A.M., Kubilay, N., Losno, R., Maenhaut, W., Paytan, A., Prospero, J.A., Shank, L.M., Siefert, R.L., 2009. Atmospheric iron deposition: global distribution, variability, and human perturbations. Annu. Rev. Mar. Sci. 1, 245–278.
Moffet, R.C., de Foy, B., Molina, L.T., Molina, M.J., Prather, K.A., 2008. Measurement of ambient aerosols in northern Mexico City by single particle mass spectrometry. Atmos. Chem. Phys. 8, 4499–4516.
Moosmüller, H., Engelbrecht, J.P., Skiba, M., Frey, G., Chakrabarty, R.K., Arnott, W.P., 2012. Single scattering albedo of fine mineral dust aerosols controlled by iron concentration. J. Geophys. Res. 117, D11210.
Ooki, A., Nishioka, J., Ono, T., Noriki, S., 2009. Size dependence of iron solubility of Asian mineral dust particles. J. Geophys. Res.-Atmos. 114, D03202.
Prahalad, A.K., Inmon, J., Dailey, L.A., Madden, M.C., Ghio, A.J., Gallagher, J.E., 2001. Air pollution particles mediated oxidative DNA base damage in a cell free system and in human airway epithelial cells in relation to particulate metal content and bioreactivity. Chem. Res. Toxicol. 14, 879–887.
Pratt, K.A., Murphy, S.M., Subramanian, R., DeMott, P.J., Kok, G.L., Campos, T., Rogers, D.C., Prenni, A.J., Heymsfield, A.J., Seinfeld, J.H., Prather, K.A., 2011. Flight-based chemical characterization of biomass burning aerosols within two prescribed burn smoke plumes. Atmos. Chem. Phys. 11, 12549–12565.
Rubasinghege, G., Lentz, R.W., Scherer, M.M., Grassian, V.H., 2010. Simulated atmospheric processing of iron oxyhydroxide minerals at low pH: roles of particle size and acid anion in iron dissolution. Proc. Natl. Acad. Sci. USA 107, 6628–6633.
Schroth, A.W., Crusius, J., Sholkovitz, E.R., Bostick, B.C., 2009. Iron solubility driven by speciation in dust sources to the ocean. Nat. Geosci. 2, 337–340.
See, S.W., Wang, Y.H., Balasubramanian, R., 2007. Contrasting reactive oxygen species and transition metal concentrations in combustion aerosols. Environ. Res. 103, 317–324.
Silva, P.J., Liu, D.Y., Noble, C.A., Prather, K.A., 1999. Size and chemical characterization of individual particles resulting from biomass burning of local Southern California species. Environ. Sci. Technol. 33, 3068–3076.
Song, X.H., Hopke, P.K., Fergenson, D.P., Prather, K.A., 1999. Classification of single particles analyzed by ATOFMS using an artificial neural network, ART-2A. Anal. Chem. 71, 860–865.
Su, Y.X., Sipin, M.F., Furutani, H., Prather, K.A., 2004. Development and characterization of an aerosol time-of-flight mass spectrometer with increased detection efficiency. Anal. Chem. 76, 712–719.
Sullivan, R.C., Guazzotti, S.A., Sodeman, D.A., Prather, K.A., 2007. Direct observations of the atmospheric processing of Asian mineral dust. Atmos. Chem. Phys. 7, 1213–1236.
Wang, J., Hu, Z.M., Chen, Y.Y., Chen, Z.L., Xu, S.Y., 2013. Contamination characteristics and possible sources of PM10 and PM2.5 in different functional areas of Shanghai, China. Atmos. Environ. 68, 221–229.

Wang, Y.S., Li, A.G., Zhang, Y.X., Xie, Y.N., Li, D.L., Li, Y., Zhang, G.L., 2006. Speciation of iron in atmospheric particulate matter by EXAFS. Chin. Sci. Bull. 51, 2275–2280.

Yan, B., Li, L., Yu, Q., Hang, W., He, J., Huang, B., 2010. High irradiance laser ionization mass spectrometry for direct speciation of iron oxides. J. Am. Soc. Mass Spectrom. 21, 1227–1234.

Yang, H., Gao, Y., 2007. Air-to-sea flux of soluble iron: is it driven more by HNO_3 or SO_2? – an examination in the light of dust aging. Atmos. Chem. Phys. Discuss. 7, 10043–10063.

Yue, W., Li, X., Liu, J., Li, Y., Yu, X., Deng, B., Wan, T., Zhang, G., Huang, Y., He, W., Hua, W., Shao, L., Li, W., Yang, S., 2006. Characterization of PM2.5 in the ambient air of Shanghai city by analyzing individual particles. Sci. Total. Environ. 368, 916–925.

Zhang, Y.P., Wang, X.F., Chen, H., Yang, X., Chen, J.M., Allen, J.O., 2009. Source apportionment of lead-containing aerosol particles in Shanghai using single particle mass spectrometry. Chemosphere 74, 501–507.

Zhuang, G., Yi, Z., Duce, R.A., Brown, P.R., 1992. Link between iron and sulphur cycles suggested by detection of Fe(n) in remote marine aerosols. Nature 355, 537–539.